Structural and Functional Analysis of the HIV gp41 Core Containing an Ile573 to Thr Substitution: Implications for Membrane Fusion[†,‡]

Jie Liu,[§] Wei Shu,[§] Melinda B. Fagan,[||] Jack H. Nunberg,[||] and Min Lu*[,§]

Department of Biochemistry, Weill Medical College of Cornell University, New York, New York 10021, and Montana Biotechnology Center, The University of Montana, Missoula, Montana 59812

Received October 25, 2000; Revised Manuscript Received December 22, 2000

ABSTRACT: The envelope glycoprotein of HIV-1 consists of the surface subunit gp120 and the transmembrane subunit gp41. Binding of gp120 to target cell receptors induces a conformational change in gp41, which then mediates the fusion of viral and cellular membranes. A buried isoleucine (Ile573) in a central trimeric coiled coil within the fusion-active gp41 ectodomain core is thought to favor this conformational activation. The role of Ile573 in determining the structure and function of the gp120−gp41 complex was investigated by mutating this residue to threonine, a nonconservative substitution in HIV-1 that occurs naturally in SIV. While the introduction of Thr573 markedly destabilized the gp41 core, the three-dimensional structure of the mutant trimer of hairpins was very similar to that of the wild-type molecule. A new hydrogen-bonding interaction between the buried Thr573 and Thr569 residues appears to allow formation of the trimer-of-hairpins structure at physiological temperature. The mutant envelope glycoprotein expressed in 293T cells and incorporated within pseudotyped virions displayed only a moderate reduction in syncytium-inducing capacity and virus infectivity, respectively. Our results demonstrate that the proper folding of the gp41 core underlies the membrane fusion properties of the gp120−gp41 complex. An understanding of the gp41 activation process may suggest novel strategies for vaccine and antiviral drug development.

Membrane glycoproteins of enveloped viruses control the key process of viral entry by mediating the attachment of the virion to target cells and the fusion of viral and cellular membranes. Envelope glycoproteins on the surface of the virion are thus major targets for the induction of protective immunity and for the development of pharmacologic interventions. The best characterized viral membrane fusion protein is the influenza virus hemagglutinin (HA).[1] In response to the mildly acidic conditions of the mature endosome, influenza fusion is activated in a process requiring complex structural changes in HA from a native (prefusogenic) to a fusogenic (fusion-active) conformation (*1*−*4*). Recent work has led to the hypothesis that the native conformation of HA is metastable; when incubated at the pH of fusion, it is transformed in a "spring-loaded" manner to an energetically more stable fusion-active state (*1*, *2*, *5*, *6*). Inhibition of this type of activation and refolding of the viral envelope protein may be central to strategies for the treatment or prevention of viral infections.

Human and simian immunodeficiency viruses (HIV and SIV) also utilize a membrane fusion event to introduce their infectious genomes into cells. The envelope glycoprotein is synthesized as a gp160 polyprotein and cleaved intracellularly to yield a noncovalent complex of the surface subunit gp120 and the transmembrane subunit gp41 (reviewed in refs *7* and *8*). Considerable evidence now indicates that the primate immunodeficiency virus entry process involves multiple steps. Upon interaction of the viral trimeric gp120−gp41 complex with cellular receptors (CD4 and members of the chemokine receptor family), the envelope glycoprotein undergoes a conformational change that allows the gp41 subunit to form the transient prehairpin intermediate in which the N-terminal fusion peptide and the transmembrane segments are anchored in the cellular and viral membranes, respectively (*9*−*12*). Subsequent helical packing interactions within gp41 resolve the prehairpin intermediate into a fusion-active hairpin structure, leading to close apposition of the two membranes for fusion (*9*, *13*, *14*). The structural consequences of these gp41 conformational changes remain imperfectly understood, in part because the native and prehairpin intermediate structures of gp41 are not known.

The structure of the gp41 ectodomain in its fusion-active state is a trimer of hairpins in which three C-terminal helices pack in an antiparallel orientation into highly conserved

[†] This work was supported by National Institutes of Health Grants AI44669 to J.H.N. and AI42382 to M.L. The work at The University of Montana was furthered by a gift from the James B. Pendleton Charitable Trust.

[‡] The refined coordinates have been deposited in the Protein Data Bank with accession number 1F23.

* To whom correspondence should be addressed: Weill Medical College of Cornell University, 1300 York Ave., New York, NY 10021. Phone: (212) 746-6562. Fax: (212) 746-8875. E-mail: mlu@mail.med.cornell.edu.

[§] Weill Medical College of Cornell University.

[||] The University of Montana.

[1] Abbreviations: HA, hemagglutinin; HIV-1, human immunodeficiency virus type 1; SIV, simian immunodeficiency virus; mAb, monoclonal antibody; HIVIG, anti-HIV immunoglobulin from infected persons; Env, envelope; $[\theta]_{222}$, molar ellipticity at 222 nm; CD, circular dichroism; HPLC, high-performance liquid chromatography; T_m, transition midpoint temperature.

10.1021/bi0024759 CCC: $20.00
Published on Web 02/10/2001

hydrophobic grooves on the outer surface of the N-terminal trimeric coiled coil (*13*, *15*−*21*). The N-terminal coiled-coil formation appears to play a critical role in initiating the gp41 refolding process leading to membrane fusion (*22*, and references therein). In the simplest model, the N-terminal heptad-repeat region exists in an non-coiled-coil conformation in the native state but forms a coiled-coil trimer in the prehairpin intermediate and fusogenic hairpin conformations (*22*−*28*). Evidence for the functional importance of this structural rearrangement comes from the finding that peptides corresponding to the C-terminal helical region are potent inhibitors of HIV-1 infection in vitro (*29*, *30*); these peptides are thought to pack into hydrophobic grooves of the N-terminal trimeric coiled coil, thereby preventing formation of the fusion-active hairpin structure (*13*, *15*−*17*). One such peptide, T-20, shows efficacy in reducing viral loads in clinical trials (*31*). Furthermore, a prominent hydrophobic cavity on the surface of the gp41 N-terminal coiled-coil core has been shown to serve as a binding pocket for small-molecule fusion inhibitors (*32*, *33*). Thus, understanding the factors that influence the folding and conformation of gp41 is likely to provide insights into the complex biology of HIV-1 entry and its inhibition.

Coiled-coil motifs share a characteristic seven-amino acid (heptad) repeat, $(abcdefg)_n$, with hydrophobic residues at the first (*a*) and fourth (*d*) positions and polar residues generally elsewhere (*34*−*36*). Sequence comparisons between HIV-1 and SIV gp41 show that residues at the *a* and *d* positions of the N-terminal heptad-repeat region are highly conserved (*37*−*39*). There is only one nonconservative substitution (Ile573 in HIV-1 and threonine in the corresponding position in SIV). Interestingly, the hydrophobicity of the side chain at position 573 markedly affects the proper folding of the gp41 core as well as the in vivo phenotypes of the gp120−gp41 complex (*23*, *28*). For example, the Ile573 to serine mutation that impedes formation of the trimer of hairpins also abolishes HIV-1 infectivity (*23*, *28*). Serine and threonine differ by a single methyl group, yet threonine is entirely functional at the corresponding position (573) in SIV gp41. This study directly tests the role of the Thr573 side chain, as opposed to those of serine and isoleucine, in conferring the structural specificity and conformational stability of the gp41 core, as well as in determining the membrane fusion activity of the HIV-1 envelope protein complex. The Ile573 to threonine substitution was found to decrease the thermal stability of the trimer of hairpins by 25 °C, relative to the wild-type molecule. In the 2.3 Å resolution crystal structure of the mutant gp41 core, the O_γ atom of Thr573 is hydrogen bonded to the Thr569 main chain CO group of the same helix, thereby forming a buried polar interaction in an otherwise hydrophobic interface between the helices. This buried polar interaction appears to allow accommodation of the polar atom of Thr573 in the hydrophobic interface of the N-terminal coiled-coil core and thus to maintain the structural integrity of the trimer of hairpins for functional gp41 activation. Indeed, the HIV-1 envelope glycoprotein bearing the Ile573 to threonine mutation exhibits only a moderate reduction in fusion activity and virion infectivity. Our studies validate the notion that the conserved coiled-coil interactions within the N-terminal heptad repeat are important determinants of the gp41 conformational change required for HIV-1 membrane fusion.

MATERIALS AND METHODS

Plasmid Constructions. Plasmids for the expression of the recombinant I573T and I573T/N36(L6)C34 model polypeptides were constructed by oligonucleotide-directed mutagenesis of plasmids pN34/C28(L6) and pN36/L34(L6), respectively (*28*, *40*). Standard protocols for DNA manipulations were followed (*41*). The Ile573 to threonine mutation was introduced into the molecularly cloned *env* gene of the HIV-1 primary isolate ACH168.10 (168P) by using QuikChange mutagenesis (Stratagene, La Jolla, CA) and verified by DNA sequencing (*42*−*44*). The expression of the HIV-1 168P envelope protein was within the context of the eukaryotic expression vector pCR-Uni 3.1 (Invitrogen) (*43*). The DNA sequence of the molecularly cloned 168P *env* (168P23) is referenced by accession number AF035532. Note that the numbering system used to denote the positions of gp41 residues in HIV-1 168P is based on the numbering of residues in HIV-1 HXB2, to facilitate comparison with structural information published for this envelope glycoprotein (*13*, *16*, *17*).

Transfection and Immunoprecipitation. FuGENE-6 reagent (Roche Molecular Biochemicals) was used to transfect human 293T cells (provided by G. Nabel, University of Michigan, Ann Arbor, MI) for transient expression (*45*). Typically, 1 μg of the HIV-1 *env* expression plasmid and 3 μL of FuGENE reagent were used, according to the manufacturer's instructions, to transfect 2×10^5 cells/well in a six-well microculture dish. Transfection efficiencies were determined by immunochemical staining of monoloayers fixed in a cold methanol/acetone mixture (1:1) using anti-HIV immunoglobulin from infected persons (HIVIG) with alkaline phosphate-conjugated goat anti-human IgG antibody (Kirkegaard and Perry Labs, Inc., Gaithersburg, MD) and PhThalo Red chromogen (Kirkegaard and Perry Labs, Inc.). The expression of the 168P *env* within the transfected cell population and on the cell surface was also assessed by Western blot analysis. Surface proteins were labeled with biotin (NHS-LC-biotin; Pierce Chemical Corp., Rockford, IL) as previously described (*45*). Cells were lysed on ice in 50 mM Tris-HCl (pH 7.5), 150 mM NaCl, and 1% Triton X-100 containing aprotinin, leupeptin, and pepstatin (1 μg/mL each), and the envelope glycoprotein was immunoprecipitated using HIVIG and protein A−Sepharose (Sigma). Western blot analysis was performed using either the gp120 V3 loop-directed mAb 50.1 (*46*) or the gp41-directed mAb Chessie 8 (*47*), and horseradish peroxidase-conjugated sheep anti-mouse IgG antibody (Cappel, West Chester, PA). The biotinylated cell surface envelope glycoprotein was detected by using the avidin−horseradish peroxidase conjugate (Biomeda Corp., Foster City, CA). Proteins were visualized by ECL detection (Amersham Pharmacia Biotech). Spontaneous and soluble CD4-induced (10 μg/mL; 1 h at 37 °C) shedding of gp120 into the supernatant of transfected cell cultures was also assessed by Western blot analysis of HIVIG immunoprecipitable protein.

Cell−Cell Membrane Fusion Assay. The ability of wild-type and mutant envelope glycoproteins to mediate cell−cell fusion was determined by coculturing env-expressing cells with U87 cells expressing CD4 and the CXCR4 coreceptor (*43*, *48*, *49*). Transfected envelope glycoprotein-expressing 293T cells and U87-CD4-CXCR4 cells were

resuspended using 0.1 mM EDTA in physiologically buffered saline (PBS), and 1×10^4 cells of each were added to a 96-well microculture dish. Cocultures were fixed and immunochemically stained after 3 and 24 h, and the percentage of envelope protein-expressing cells involved in syncytium formation was determined microscopically.

Generation and Characterization of Pseudotyped Virions. HIV-1 virions containing the wild-type or mutant envelope glycoprotein were constructed by cotransfection of human 293T cells with the env-expressing plasmid and the *env*-defective proviral plasmid pSVNLthyDBgl (*43*, *50*). This latter plasmid contains the HIV NL4-3 provirus with a *Bgl*I−*Bgl*I deletion of the *env* gene. Cells were transfected using a 1:1 ratio of the HIV-1 168P *env* plasmid and pSVNLthyDBgl DNAs and FuGENE reagent (total of 1 μg of DNA and 3 μL of FuGENE-6 reagent for 2×10^5 cells per well in a six-well microculture dish). Transfection and harvest conditions were optimized using the wild-type 168P *env* plasmid. Three days post-transfection, cell culture supernatants containing pseudovirions were collected, filtered (0.22 μm), and used without freezing. The relative amount of envelope glycoprotein incorporated within wild-type and mutant pseudovirions was determined by analysis of pelleted particles purified by centrifugation (*51*, *52*). The envelope glycoprotein was quantitated by Western blot analysis using the gp120 V3-directed mAb 50.1 as described above, except that ECL-Plus (Amersham Pharmacia Biotech) was used and specific chemifluoresence was determined using a Fuji FLA-3000G analyzer. The relative amount of p24 was similarly quantified using HIVIG to identify pseudovirion p24 (*45*). The infectivity of pseudovirion-containing supernatant was determined by the enumeration of infected U87-CD4-CXCR4 cells in 96-well microcultures (*43*, *48*). The number of infected foci was determined 2 days after infection by immunochemical staining of cultures fixed in a methanol/acetone mixture using HIVIG, as described above.

Protein Production and Purification. All recombinant polypeptides were expressed in *Escherichia coli* BL21(DE3)/pLysS using the T7 expression system (*53*). Cells, freshly transformed with an appropriate plasmid, were grown to late log phase. Protein expression was induced by addition of 0.5 mM isopropyl thio-β-D-galactoside (IPTG). After an additional 3 h of growth at 30 or 37 °C, the bacteria were harvested by centrifugation, and the cells were lysed with glacial acetic acid as described previously (*54*). Proteins were purified from the soluble fraction to homogeneity by reverse-phase HPLC (Waters) with a Vydac C-18 preparative column using a water/acetonitrile gradient in the presence of 0.1% (v/v) trifluoroacetic acid. The peptide identity was confirmed by matrix-assisted laser-desorption ionization mass spectrometry (PerSeptive Biosystems Voyage Elite). Protein concentrations were determined by measuring the absorbance at 280 nm in 6 M guanidinium hydrochloride (*55*).

Circular Dichroism Spectroscopy. CD spectra were acquired on an AVIV 62DS circular dichroism spectrometer with a thermoelectric sample temperature controller. Samples for wavelength spectra were 10 μM peptide in 50 mM sodium phosphate (pH 7.0) and 150 mM NaCl. The cuvette path length was 0.1 cm. The wavelength dependence of molar ellipticity, [θ], was monitored at 0 °C as the average of five scans, using a 5 s integration time at 1.0 nm wavelength increments. Spectra were baseline-corrected against the cuvette with buffer alone. The fractional helix content was calculated from the CD signal by dividing the mean residue ellipticity at 222 nm by the value expected for 100% helix formation by helices of comparable size, −33000 deg cm^2 dmol^{-1} (*56*). Thermal stability was determined in the same buffer by measuring $[\theta]_{222}$ as a function of temperature. A 1.0 cm path length cell was used with continuous stirring. Thermal melts were monitored in 2 °C intervals with a 2 min equilibration at the desired temperature, and an integration time of 30 s. Reversibility was checked by repeated scans. The thermal melt of I573T was not reversible, while that of I573T/N36(L6)C34 was reversible with superimposable folding and unfolding curves and >90% of the signal regained upon cooling. The midpoint of the thermal unfolding transition (T_m) was determined from the maximum of the first derivative, with respect to the reciprocal of the temperature, of the $[\theta]_{222}$ values (*57*). The error in the estimation of T_m is ±1 °C.

Sedimentation Equilibrium. Apparent molecular weights were determined by sedimentation equilibrium studies with a Beckman XL-A Optima analytical ultracentrifuge as described previously (*58*). Protein samples were dialyzed overnight against 50 mM sodium phosphate (pH 7.0) and 150 mM NaCl, loaded at initial concentrations of 10, 30, and 100 μM, and analyzed at 20 °C at rotor speeds of 20 000 and 23 000 rpm for I573T, and 17 000 and 20 000 rpm for I573T/N36(L6)C34. Data were acquired at two wavelengths per rotor speed and processed simultaneously with a nonlinear least-squares fitting routine (*59*). Solvent density and protein partial specific volume were calculated according to solvent and protein composition, respectively (*60*). Molecular weights were all within 10% of those calculated for an ideal trimer, with no systematic deviation of the residuals.

Crystallization, Data Collection, and Structure Determination. The I573T/N36(L6)C34 mutant was crystallized by the hanging-drop vapor diffusion method at room temperature. To grow crystals, a 10 mg/mL HPLC-purified protein stock was diluted 1:1 with a reservoir and allowed to equilibrate against the reservoir solution. Initial crystallization conditions were screened by using sparse matrix crystallization kits (Crystal Screen I and II, Hampton Research, Riverside, CA) and then optimized. Crystals of I573T/N36(L6)C34 in space group *P*1 were grown from 0.1 M sodium citrate (pH 4.6), 5% propanol, and 7% polyethylene glycol 4000. For data collection, crystals were transferred to a cryoprotected solution containing 15% (v/v) glycerol in the corresponding mother liquor. Diffraction data were collected at 95 K using an R-axis IV image plate detector mounted on a Rigaku RU200 rotating anode X-ray generator at the X-ray Crystallography Facility at the Weill Medical College of Cornell University. Diffraction intensities were integrated by using DENZO and SCALEPACK software (*61*) and reduced to structural factors with the program TRUNCATE from the CCP4 program suite (*62*).

The structure of I573T/N36(L6)C34 was determined by molecular replacement using the program AMoRe (*63*). The 2.4 Å X-ray structure of the N34(L6)C28 trimer was used as a search model (*17*). The initial model was built by using conventional $(2F_o - F_c)\Phi_{calc}$ and $(F_o - F_c)\Phi_{calc}$ maps at 3.0 Å. Overall anisotropic *B*-factor and bulk solvent corrections were applied. Many cycles of torsional angle simulated annealing and grouped *B*-factor refinement (*64*) were fol-

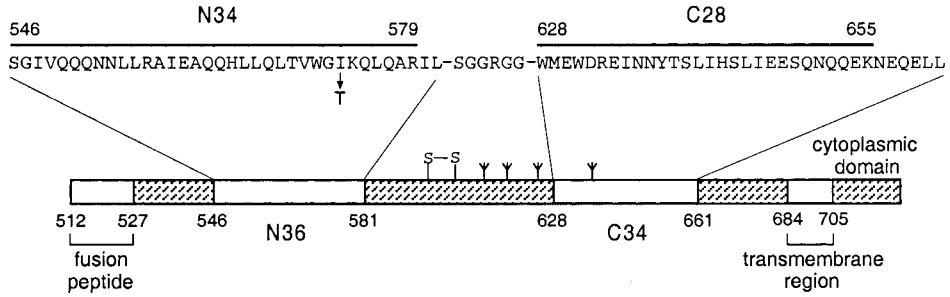

FIGURE 1: Schematic view of the HIV-1 gp41 envelope glycoprotein. The important functional features of the gp41 ectodomain, the peptides identified by protein dissection, and the sequences of N36 and C34 are shown. The N36(L6)C34 model consists of N36 and C34 plus a six-residue linker. The Thr573 to threonine substitution is indicated below the N36 sequence. The disulfide bond and four potential N-glycosylation sites are depicted. The residues are numbered according to their position in gp160 of the HXB2 HIV-1 strain.

lowed by extensive rebuilding. The resulting map revealed traceable electron density for all the amino acid residues except for a few at the helix termini and in the linker region. The final model corresponding to two trimers was built with the program O (*65*). The structure was refined by using positional and *B*-factor refinements (*64*) for all data between 50.0 and 2.3 Å resolution. Crystallographic refinement of the structure was carried out with the program CNS 0.5 (*66*). As the refinement proceeded, 271 waters were added. Model geometry was analyzed by PROCHECK (*67*), with all residues but a few at the helix termini and in the linker region occupying most-preferred regions of the Ramachandran space. Ala578 of monomers A and B, Leu660 of monomer B, Ile580 and Ser1 of monomer D, and Leu581 and Glu659 of monomer E lie in the additionally allowed regions of the Ramachandran plot. The overall temperature factor of the model is 28.5 Å^2. Side chains of Arg579 of monomers A and F, Arg4 of monomers A−C and E, Met629 and Arg633 of monomer B, Glu659 of monomers C and F, Glu654 of monomer E, and Gln577 and Gln658 of monomer F are disordered and were thus modeled as serine. Side chains of Met629 of monomer A, Gln550, Arg579, Ile580, and Lys655 of monomer B, Gln577, Arg579, His643, Asn651, and Gln658 of monomer C, His643, Glu654, and Gln658 of monomer D, Lys655 and Gln658 of monomer E, and Ile580 and Lys655 of monomer F were modeled as alanine, while side chains of Leu581 and Ser1 of monomer A were modeled as glycine. In addition, Ile580 of monomer A, Leu581 of monomers B and C, Ser1, Gly2, and Gly3 of monomers B, C, and F, and Leu661 of monomers A and C−E were left out of the model because of the absence of interpretable electron density for these atoms.

RESULTS

gp41 Ectodomain Core with Buried Thr573 Residues. The Ile573 residue, located at an *a* heptad position in the N-terminal heptad-repeat region of gp41, is completely conserved in 208 of 213 fully sequenced M group HIV-1 strains (*68*). All the remaining five isolates at this position possess a conservative valine substitution. Mutagenesis studies have shown that nonconservative substitutions for Ile573 abolish infectivity and membrane fusion (*23*) and cause a folding defect in the recombinant N34(L6)C26 polypeptide model for the gp41 ectodomain core (*28*). Thus, the high level of sequence conservation of the buried isoleucine residue is thought to result from selective pressure to maintain the trimeric coiled-coil interactions within the fusogenic gp41 conformation needed for initiating HIV-1 membrane fusion. It is therefore puzzling that SIV gp41 contains the polar threonine residue at the corresponding position. To address how this nonconservative mutation affects the folding of HIV-1 gp41, we substituted Ile573 with threonine in N34(L6)C28 (Figure 1). This mutant recombinant polypeptide, named I573T, was produced by bacterial expression and purified by reverse-phase high-performance liquid chromatography.

Sedimentation equilibrium measurements were used to determine the oligomerization state of the I573T mutant. Like the wild-type peptide, I573T sediments as a discrete trimer over a 10-fold range of peptide concentrations (10−100 μM) (Figure 2a and Table 1). On the basis of circular dichroism measurements at a protein concentration of 10 μM in 50 mM sodium phosphate (pH 7.0) and 150 mM NaCl at 0 °C, I573T contains >95% α-helical structure, whereas the same recombinant peptide with the fusion-defective serine mutation (I573S) appears to be ∼40% helical (Figure 2b and Table 1). Under these conditions, I573T exhibits a cooperative thermal unfolding transition with an apparent melting temperature (T_m) of 45 °C, as compared to the apparent T_m value of 70 °C for N34(L6)C28 (wild-type) (Figure 2c and Table 1). The I573T trimeric structure is less stable than the wild-type molecule, yet it is considerably more stable than the corresponding I573S mutant (Table 1). This reinforces the observation that buried polar residues in the hydrophobic core of a coiled coil are generally destabilizing (e.g., ref *69*). Nevertheless, it would appear that the I573T mutant can fold into a stable trimer-of-hairpins structure at physiological temperature.

To better understand how the buried threonine side chain influences the folding and stability of the gp41 core, we determined the X-ray crystal structure of the trimeric gp41 core containing the Ile573 to threonine mutation at 2.3 Å resolution. We were unable to obtain crystals of the I573T mutant in the N34(L6)C28 model and so made use of the slightly larger N36(L6)C34 model (*70*) (see Figure 1). Crystals of I573T/N36(L6)C34 have distinct, triclinic symmetry and contain six monomers in the asymmetric unit; each monomer is related by an approximate noncrystallographic 3-fold axis. Using the molecular replacement method, an initial model corresponding to two trimers was built. Iterative rounds of manual rebuilding and refinement increased the quality of the initial electron density map and served to reduce model bias, as guided chiefly by improvement in the free *R*-factor. The structure has been refined to a conventional

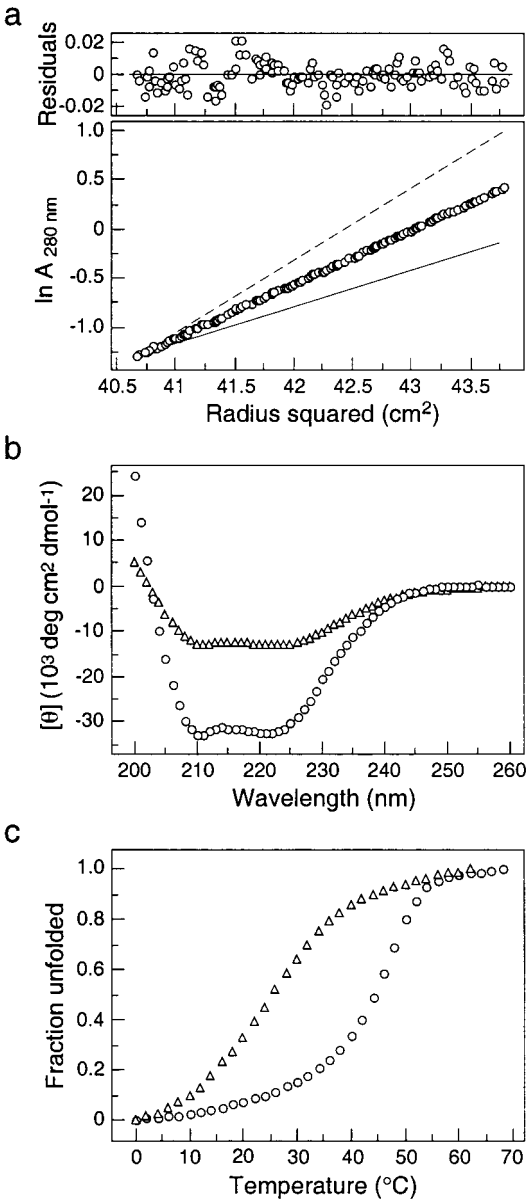

FIGURE 2: Folding of the I573T peptide as an α-helical trimer. (a) Sedimentation equilibrium data (20 000 rpm) of I573T collected at 20 °C in 50 mM sodium phosphate (pH 7.0) and 150 mM NaCl at a protein concentration of ~30 μM. The natural logarithm of the absorbance at 280 nm is plotted against the square of the radial position. The random distributions of the residuals indicate that the data fit well to an ideal single-species model. The slope of the plotted data indicates the I573 peptide is a trimeric species. The calculated data for dimeric and tetrameric models are indicated by solid and dashed lines, respectively. (b) Circular dichroism (CD) spectra of I573T (○) and I573S (△) at 0 °C in 50 mM sodium phosphate (pH 7.0) and 150 mM NaCl at a protein concentration of 10 μM. (c) Thermal melts monitored by CD at 222 nm for I573T (○) and I573S (△). The decrease in the fraction of a folded molecule is shown as a function of temperature.

R-factor of 19.1% and a free *R*-factor of 27.0% for data in the resolution shell from 50.0 to 2.3 Å. The root-mean-square deviations of bond lengths and bond angles from the ideal values are 0.006 Å and 0.9°, respectively. The final $2F_o - F_c$ electron density map is of good quality (Figure 3a) and reveals the positions of all amino acid residues except for a few disordered residues at the helix termini and in the six-residue loop region (see Materials and Methods). The crystallographic statistics are summarized in Table 2.

Table 1: Summary of Circular Dichroism and Sedimentation Equilibrium Data for the HIV-1 gp41 Core Mutants

model	$-[\theta]_{222}$[a] (deg cm^2 dmol^{-1})	T_m[a] (°C)	molecular mass (kDa)
N34(L6)C28	31 300	70	24.4
I573S	13 100	25	NA[b]
I573T	32 300	45	24.1

[a] All scans and melts were performed at a protein concentration of 10 μM. [b] NA, not applicable. The I573S peptide forms an insoluble aggregate at concentrations above ~10 μM in 50 mM sodium phosphate (pH 7.0) and 150 mM NaCl.

The overall architecture and helix packing of the I573T/N36(L6)C34 trimer are the same as those of the wild-type gp41 core (*13*, *16*, *17*). Three molecules, each consisting of an N36 helix paired with an antiparallel C34 helix, pack together around the noncrystallographic 3-fold axis to form a trimer of hairpins. Three N36 helices form an interior, parallel coiled-coil trimer with a left-handed superhelical pitch, while three C34 helices wrap in an oblique, antiparallel manner against the surface of the N36 coiled coil (Figure 3b). The root-mean-square (rms) deviation between all C_α atoms of the entire helical regions between I573T/N36(L6)C34 and the wild-type N36/C34 complex (*16*) is 0.54 Å. This correspondence indicates that the Thr573 substitution causes little distortion of the trimer-of-hairpins structure. In addition, comparatively weak electron density and higher-than-average main chain *B*-values suggest that the Ser-Gly-Gly-Arg-Gly-Gly hydrophilic linker of the I573T/N36(L6)C34 mutant may be dynamically disordered. Thus, the linker does not dominate formation of the trimer of hairpins.

In both wild-type and I573T/N36(L6)C34 structures, three N helices are packed together in the classical acute "knobs-into-holes" arrangement characteristic of trimeric coiled coils, in which the $C_\alpha - C_\beta$ bonds in the side chains (knobs) of residues *a* and *d* make an acute angle with respect to the recipient holes formed by spaces between four residues on the neighboring helices (*69*, *71*). The Thr573 side chains, at the *a* position, face each other across the molecular 3-fold symmetry axis and form a network of new hydrogen bonds between the side chain O_γ atom and the backbone carbonyl group of Thr569 in the preceding turn of the same helix (Figure 4). As a consequence, a cavity (22 Å^3) is located between the Thr569 and Thr573 layers. No electron density was apparent in this cavity. The Thr573 side chains move closer to each other toward the center of the coiled-coil trimer. The radius of the coiled-coil core at this Thr573 layer, calculated on the basis of the average $C_\alpha - C_\alpha$ distance between the residues at the same heptad layer, is 3.79 Å. In contrast, the radius of the corresponding Ile573 layer in the wild-type N36/C34 structure is 3.94 Å. It would appear that the stabilization energy gained from the favorable hydrogen-bonding and side chain packing interactions allows the polar threonine residues to be accommodated in the interior coiled-coil core without significantly altering the trimer-of-hairpins structure. In addition, the C_γ atoms of the Thr573 side chains are too far from each other to make van der Waals contacts and the buried Thr573 residue therefore contributes little to the interhelical packing interactions.

Membrane Fusion Properties of the I573T Envelope Glycoprotein. Replacement of the buried Ile573 residue by either serine, glycine, or proline completely inhibits the abil-

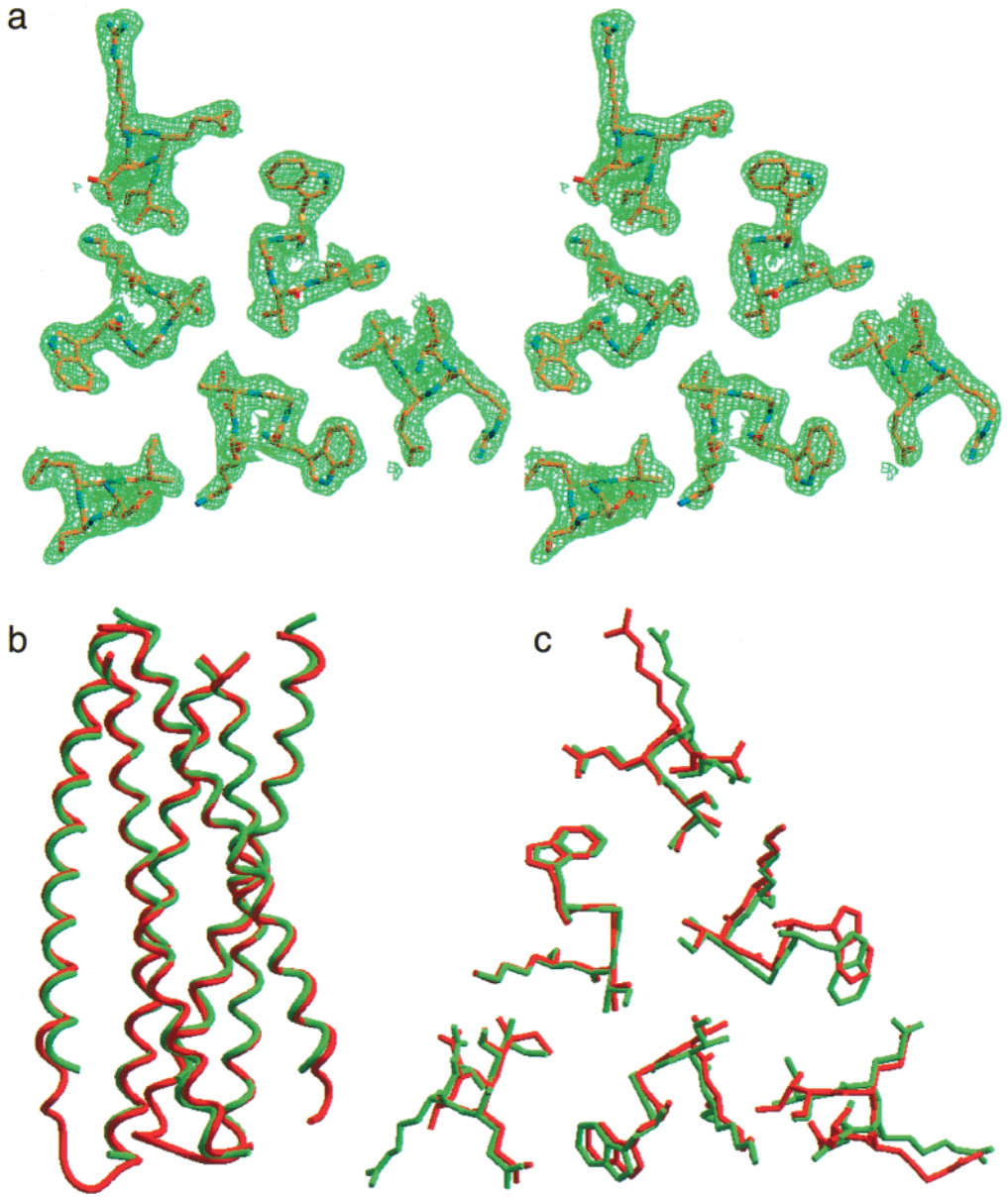

FIGURE 3: Crystal structure of the I573T/N36(L6)C34 trimer. (a) Stereoview of the final electron density map at 2.3 Å resolution, contoured at 1.0 standard deviation above the average density. The acute knobs-into-holes packing of Thr573 in an *a* level is shown. (b) Side view of the C_α traces of the N36 and C34 helices in the N36/C34 complex (green) and I573T/N36(L6)C34 (red) structures which were used for the superposition. The N-terminus of N36 and the C-terminus of C34 are at the top of the figure. (c) A cross section of the helix packing near the Thr573 layer. Structures of N36/C34 (green) and I573T/N36(L6)C34 (red) are overlaid. The figures were generated with the program SETOR (*82*).

ity of the envelope glycoprotein to mediate membrane fusion and also disrupts formation of the trimeric N34(L6)C28 complex (*23*, *28*). The structure and folding of the gp41 core is thus believed to control the key process of HIV-1 membrane fusion (*22*, *28*). Therefore, a mutation that affects the stability of the trimer-of-hairpins structure would be predicted to change the fusion properties of the HIV-1 envelope glycoprotein. Since the I573T mutant clearly maintains the trimer-of-hairpins structure, albeit with less thermal stability, we asked whether the threonine mutation would also affect the membrane fusion activity of the gp120−gp41 complex. To test this, we introduced the Ile573 to Thr mutation into the intact envelope glycoprotein of the HIV-1 primary isolate ACH168.10 (168P). This dual coreceptor-utilizing primary isolate has been well-characterized (*42*, *44*), and the molecularly cloned *env* gene has been used in other studies of envelope glycoprotein biology (*43*, *45*, *72*). The gp41 subunit of the 168P envelope glycoprotein is identical to the wild-type N34(L6)C28 in amino acid sequence throughout the N34 region and at all *a* and *d* positions of the C28 helix.

In keeping with the minimal structural changes induced by the Ile573 to threonine mutation characterized above, we could detect no differences in the biosynthesis of the wild-type 168P and I573T envelope glycoproteins when expressed in human 293T cells. Transient transfection studies yielded comparable frequencies and levels of envelope glycoprotein expression. Furthermore, envelope glycoprotein processing and transport to the cell surface were also comparable, as determined by Western blot analysis of cell surface-expressed gp160 and gp120 (Figure 5a). In both cases, ~30% of the cell surface envelope protein was found as mature, pro-

Table 2: X-ray Data Collection and Refinement Statistics

unit cell dimensions	
a, *b*, *c* (Å)	38.92, 41.87, 55.98
α, *β*, *γ* (deg)	90.59, 88.93, 96.28
space group	*P*1
data processing	
resolution (Å)	50.0−2.3
no. of measured reflections	62249
no. of unique reflections	14667
completeness (%)	96.1
R_{merge}[a] (%)	7.6
refinement	
resolution (Å)	50.0−2.3
no. of reflections in the working set	13174
no. of reflections in the test set	1493
no. of protein non-hydrogen atoms	3494
no. of water molecules	271
R_{free}[b] (%)	27.0
R_{cryst}[b] (%)	19.1
average *B*-factor (Å^2)	28.5
rms deviations from ideality	
bond lengths (Å)	0.006
bond angles (deg)	0.9
torsion angles (Å)	15.9

[a] $R_{merge} = \Sigma|I - \langle I\rangle|/\Sigma I$, where I is the intensity of an individual measurement and $\langle I\rangle$ is the average intensity from multiply recorded reflections. [b] $R_{cryst} = \Sigma|F_{obs} - F_{calc}|/\Sigma F_{obs}$, where F_{obs} and F_{calc} are the observed and calculated structural factors, respectively. No σ cutoff was applied. R_{free} is calculated for a set of reflections that were excluded from refinement.

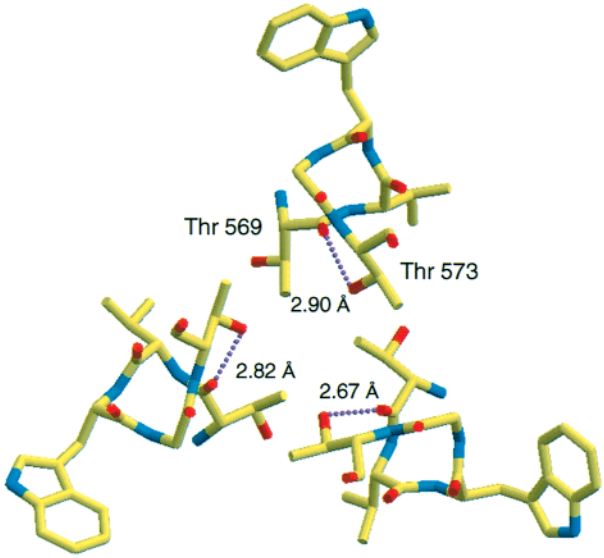

FIGURE 4: Thr573 side chain hydrogen bonding to the Thr569 carbonyl group in the I573T/N36(L6)C34 structure. Oxygen, nitrogen, and carbon atoms are colored red, blue, and yellow, respectively. The hydrogen bond is shown as a purple dotted line. This figure was created with the program SETOR (*82*).

teolytically processed gp120. The accumulation of unprocessed (and fusion-inactive) gp160 presumably reflects saturation of the cellular proteolytic machinery in the context of high levels of envelope protein expression. Examination of the cell culture supernatants from transfected cells also revealed comparable levels of spontaneously shed wild-type 168P and I573T gp120 (Figure 5a). Incubation with soluble CD4 did not significantly increase the amount of gp120 shedding above this level. Thus, the wild-type and I573T envelope glycoproteins were indistinguishable in their biosynthesis transport and processing.

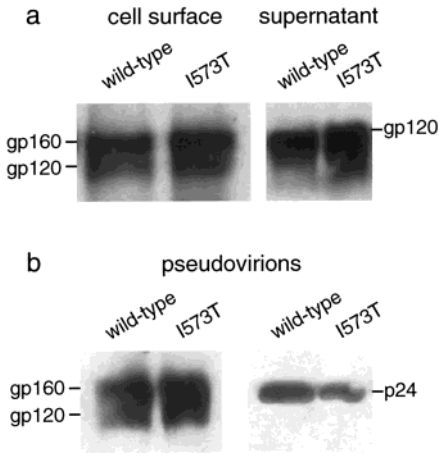

FIGURE 5: Analysis of envelope glycoprotein expression and incorporation into pseudotyped virions. (a) Western blot analysis of wild-type and I573T envelope glycoprotein expression in transfected 293T cells. The cell surface envelope glycoprotein (left) was identified by surface biotinylation as described in Materials and Methods. Shed gp120 was identified in the cell culture supernatant (right) using mAb 50.1. (b) Western blot analysis of centrifugally purified pseudotyped virion particles containing wild-type and I573T envelope glycoprotein. The virion envelope glycoprotein (left) was identified as described using mAb 50.1. The virion p24 core antigen (right) was identified using HIVIG.

The ability of the wild-type and I573T envelope glycoproteins to mediate cell−cell fusion was assessed by coculture of envelope glycoprotein-expressing 293T cells with human U87 glioma cells expressing both CD4 and the CXCR4 coreceptor (U87-CD4-CXCR4) (*43*, *48*, *49*). Envelope glycoprotein-induced cell−cell fusion was assessed microscopically at 3 and 24 h following mixing of the cells. The I573T mutant envelope glycoprotein was entirely competent in inducing multinucleated syncytium formation. In most experiments, however, the I573T mutant yielded a slightly lower percentage of envelope glycoprotein-expressing cells in syncytia and a smaller number of nuclei per syncytia at the 24 h time point (typically 10−20 nuclei/syncytium vs 30−50 nuclei/syncytium in the wild type) (Figure 6). Syncytium formation could be inhibited by incubation with soluble CD4, and both envelope glycoproteins were similarly sensitive to this inhibition, with an IC_{50} (50% inhibitory concentration) of ∼100 μg/mL. Thus, and in striking contrast to the previously published I573S mutant envelope glycoprotein (*23*), the I573T protein appears only slightly reduced in its ability to mediate membrane fusion.

Infectivity of HIV-1 Virions Bearing the I573T Envelope Glycoprotein. To test the ability of the I573T mutant envelope glycoprotein to mediate virus−cell fusion and to initiate infection, we generated pseudotyped virion particles bearing the wild-type and I573T envelope glycoproteins. These pseudotyped viruses were produced by cotransfection of 293T cells with a plasmid expressing the respective envelope glycoprotein and a plasmid expressing an otherwise-infectious HIV NL4-3 provirus genome but with a deletion in the *env* gene (*43*, *50*). Particles comprising the NL4-3 core and the respective envelope glycoprotein were harvested from the culture supernatant and contained comparable amounts of virion p24 core antigen (Figure 5b). In addition, both wild-type and I573T envelope glycoproteins were incorporated into virion particles with comparable efficien-

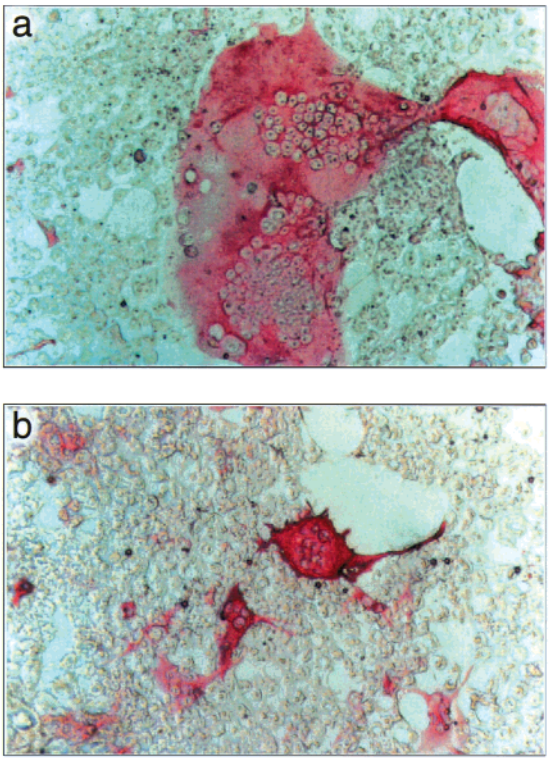

FIGURE 6: Syncytium formation by the wild-type and I573T envelope glycoprotein. 293T cells were transfected to transiently express the wild-type or I573T envelope glycoprotein and were cocultured with U87-CD4-CXCR4 target cells for 24 h to assess envelope glycoprotein-mediated cell−cell fusion. The microphotograph demonstrates the functionality of the I573T envelope glycoprotein (b), as well as the slight reduction in the ultimate extent of multinucleated cell (syncytium) formation relative to the wild-type glycoprotein (a). Envelope protein-expressing cells are stained in red.

cies, as determined by the ratio of the envelope glycoprotein to the p24 gag core protein in centrifugally purified particles (Figure 5b). As on the cell surface, mature gp120 comprised only a fraction of the total virion envelope protein. Both wild-type and I573T pseudotyped particles yielded infectious virus. Viral titers were determined by titration of pseudotyped virus stocks onto U87-CD4-CXCR4 cells. In these studies, high concentrations of transfected cell supernatant-containing pseudotyped virus (≤1:10 dilution of supernatant onto target cells) exhibited an unexplained inhibitory effect on infectivity. The nominal titer of infectious wild-type and I573T pseudotyped virions was therefore determined at greater dilutions where the number of foci of infected cells was linearly related to the virus input (Figure 7). This analysis suggests that the infectivity of pseudotyped virions bearing the I573T mutant envelope glycoprotein is not markedly reduced relative to pseudotyped virions bearing the wild-type envelope glycoprotein. It should be noted that the precise interpretation of pseudotyped virion titer is confounded by variability among transfection experiments and by the high level of uncoordinated synthesis and assembly of virion particles in this system. The slight reduction observed in viral infectivity in the I573T virion corresponds with the previously noted reduction in the ability of the I573T envelope glycoprotein to mediate cell−cell fusion, and perhaps with the moderate reduction in the thermal stability of the I573T gp41 core.

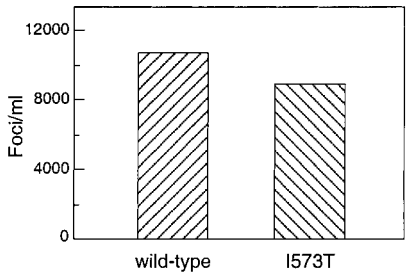

FIGURE 7: Infectivity of pseudotyped virions bearing wild-type or I573T envelope glycoprotein. Pseudotyped virions were prepared as described, and assayed for infectivity using U87-CD4-CXCR4 cells. Infectious titer of pseudovirions per milliliter of transfected cell supernatant. Nominal titers were calculated using data from the 1:16 dilution.

DISCUSSION

Evidence suggests that the HIV-1 envelope glycoprotein can adopt at least three different conformations: the native state, the prehairpin intermediate, and the fusogenic state (reviewed in refs *12* and *73*). This structural polymorphism is the means whereby the gp41 molecule is activated to drive membrane fusion during viral entry. The structural and biophysical properties of a proteolytically resistant ectodomain of HIV-1 gp41 in the putative fusogenic state are well-characterized (*13*, *15*−*17*, *28*, *54*, *74*). Three gp41 molecules form a trimer of hairpins in which an N-terminal three-stranded coiled coil is surrounded by a sheath of three antiparallel C-terminal helices. Earlier genetic studies showed that conservative changes (leucine or valine) in the Ile573 site (an *a* position in the gp41 N-terminal heptad-repeat region) maintain a wild-type fusion phenotype, while non-conservative mutations (serine or proline) result in the envelope glycoproteins that are completely defective in mediating membrane fusion (*23*). Interestingly, a correlation is observed between mutational effects on the thermal stability of the N34(L6)C28 trimer and on the membrane fusion activities of the intact envelope glycoprotein (*28*). It would appear that the free energy made available by the assembly of the fusogenic gp41 core complex is required to bring two lipid bilayers into intimate approximation to initiate fusion (*9*, *12*−*14*). In a similar manner, triggering N-terminal trimeric coiled-coil formation at an early step of the gp41 activation process is postulated to provide a thermodynamic driving force for its initial structural rearrangements toward the prehairpin intermediate, though few details are understood (*22*, *26*, *28*). This conformational change likely facilitates exposure of the hydrophobic, glycine-rich sequence termed the fusion peptide at the N-terminus of gp41, leading to insertion into the bilayer of the target membrane to bridge the two membranes at the fusion site (*1*, *2*, *75*, *76*).

The N-terminal heptad-repeat sequence of gp41 is one of the most highly conserved regions within the HIV-1 envelope glycoprotein, a protein noted for its diversity among even closely related isolates (*37*−*39*). When HIV and SIV gp41 are compared, 10 of 15 residues at the *a* and *d* positions are identical, with a single nonconservative substitution (Ile573 to threonine) present at an *a* position. This high degree of sequence conservation supports the proposal that the hydrophobicity of the substituted residue at position 573 is critical for refolding of gp41 into its fusogenic conformation during membrane fusion. The presence of a polar threonine residue

at this site in SIV gp41 raises questions about this proposal. In this study, we have analyzed the structural role of the Thr573 residue on the folding and stability of the HIV-1 gp41 core. Thermal unfolding experiments indicate that the Ile573 to threonine mutation leads to a destabilization of the trimer-of-hairpins structure by a T_m shift of ~25 °C, with a T_m value of 45 °C for the I573T mutant. By comparison, the fusion-defective Ile573 to serine mutation essentially disrupts the formation of the gp41 core structure (Table 1). The crystal structure of the I573T/N36(L6)C34 mutant at 2.3 Å resolution shows that the buried Thr573 residue is accommodated in the trimer of hairpins, and that the O_γ atom of Thr573 is able to form a new hydrogen bond with the main chain CO group of Thr569 of the same helix. Consequently, the polar atoms of the threonines are inaccessible to solvent, thereby allowing them to pack efficiently in the coiled-coil trimer interface. Indeed, the same buried intrahelical hydrogen bond is formed between Thr569 and the invariant Thr573 residue in the SIV N36/C34 trimer (*19*). Interestingly, in the case of SIV, the replacement of Thr573 with isoleucne further increases the T_m of the trimeric SIV N34(L6)C28 complex from 48 to 69.6 °C, a value close to that of the analogous HIV-1 wild-type molecule (*77*). Therefore, we infer that the buried core residue at position 573 (threonine in SIV vs isoleucine in HIV-1) is responsible for a thermal stability difference between the HIV-1 and SIV gp41 cores. This stability difference may be related to known phenotypic differences between HIV-1 and SIV envelope glycoproteins (*22*, and references therein). For example, it has been reported that the gp120 and gp41 subunits associate more tightly in SIV than in HIV-1 (*78*, *79*). One might envision that this association is strengthened not by stabilization of the native gp120−gp41 complex but rather by the relative destabilization of the fusion-active core of SIV gp41 by the Thr573 side chain.

Our biophysical and structural analyses directly demonstrate that the gp41 ectodomain core with the Ile573 to threonine mutation is stably folded under physiological conditions, even though it is destabilized relative to the wild-type molecule. If the stability of fusion-active gp41 is an important determinant for its fusion potential (*22*, *28*), one might expect the mutant HIV-1 envelope glycoprotein to be functional, albeit perhaps with some impairment in fusion efficiency. Consistent with this prediction, we have shown that the fusion phenotype of the I573T envelope glycoprotein is similar to that of the wild-type envelope protein complex. When assayed for the ability to drive cell−cell fusion, the mutant envelope glycoprotein induces multinucleated syncytia that are only slightly less extensive than those produced by the wild-type glycoprotein. Infectivity studies using pseudotyped virions also show that the mutant virion infects U87 cells with only slightly reduced titer, relative to the wild type. By contrast, the gp120−gp41 complex bearing the highly destabilized Ile573 to serine mutation is defective in mediating membrane fusion (*23*, *28*). Our results provide direct evidence that the stability of the trimer-of-hairpins structure determines the membrane fusion properties of the gp120−gp41 complex. We propose that the receptor-triggered conformational changes of the HIV-1 envelope glycoprotein are thermodynamically controlled, and that the process of membrane apposition and lipid bilayer fusion is driven by the currency of energy released from the formation of the fusion-active gp41 core. We suggest that the conformational state and membrane fusion activity of the gp120−gp41 complex are mechanistically coupled and thermodynamically linked.

A major problem in the development of envelope protein immunogens for HIV-1 vaccines is the lack of information about the antigenic structure of the functioning envelope glycoprotein. Recent studies suggest that the transiently populated intermediate structures within the gp120−gp41 complex are able to elicit broadly neutralizing antibodies (*72*). An understanding of the structural determinants for the native and intermediate conformations of the HIV-1 envelope protein will thus have ramifications beyond general considerations of the biology of viral entry and will be critical in the rational design of potential vaccine immunogens. It is possible, as perhaps in SIV, that introducing mutations to destabilize the HIV-1 N-terminal trimeric coiled-coil interactions within the prehairpin intermediate could block gp41 activation and shift the conformational equilibrium of the envelope protein toward the native state. Efforts to preserve the native envelope glycoprotein structure in vaccine candidates have to date relied on approaches to stabilize the trimeric gp120−gp41 complex (*80*, *81*). Alternatively, mutations such as those at position 573 that destabilize the fusogenic gp41 hairpin structure may result in an increased population of the postulated prehairpin intermediate. The data presented here suggest that the analysis of gp41 ectodomain core mutants may offer a test bed for the definition of the gp41 conformational states and may allow the stabilization of either the native gp120−gp41 complex or intermediate structures. Emerging structural, biophysical, and blological information will provide insights to guide the development of effective HIV vaccines and antiviral agents.

REFERENCES

1. Carr, C. M., and Kim, P. S. (1993) *Cell 73*, 823−832.
2. Bullough, P. A., Hughson, F. M., Skehel, J. J., and Wiley, D. C. (1994) *Nature 371*, 37−43.
3. Huguson, F. M. (1995) *Curr. Biol. 5*, 265−274.
4. Hernandez, L. D., Hoffman, L. R., Wolfsberg, T. G., and White, J. M. (1996) *Annu. Rev. Cell Dev. Biol. 12*, 627−661.
5. Chen, J., Wharton, S. A., Weissenhorn, W., Calder, L. J., Hughson, F. M., Skehel, J. J., and Wiley, D. C. (1995) *Proc. Natl. Acad. Sci. U.S.A. 92*, 12205−12209.
6. Carr, C. M., Chaudhry, C., and Kim, P. S. (1997) *Proc. Natl. Acad. Sci. U.S.A. 94*, 14306−14313.
7. Hunter, E., and Swanstrom, R. (1990) *Curr. Top. Microbiol. Immunol. 157*, 187−253.
8. Luciw, P. A. (1996) in *Fields Virology* (Fields, B. N., Knipe, D. M., Howley, P. M., Chanock, R. M., Melinick, J. L., Monath, T. P., Roizman, B., and Straus, S. E., Eds.) pp 1881−1952, Lippincott-Raven Publishers, Philadelphia.
9. Furuta, R. A., Wild, C. T., Weng, Y., and Weiss, C. D. (1998) *Nat. Struct. Biol. 5*, 276−279.
10. Jones, P. L., Korte, T., and Blumenthal, R. (1998) *J. Biol. Chem. 273*, 404−409.
11. Munoz-Barroso, I., Durell, S., Sakaguchi, K., Appella, E., and Blumenthal, R. (1988) *J. Cell Biol. 140*, 315−323.
12. Chan, D. C., and Kim, P. S. (1998) *Cell 93*, 681−684.
13. Weissenhorn, W., Dessen, A., Harrison, S. C., Skehel, J. J., and Wiley, D. C. (1997) *Nature 387*, 426−430.
14. Hughson, F. M. (1997) *Curr. Biol. 7*, R565−R569.
15. Lu, M., Blacklow, S. C., and Kim, P. S. (1995) *Nat. Struct. Biol. 2*, 1075−1082.
16. Chan, D. C., Fass, D., Berger, J. M., and Kim, P. S. (1997) *Cell 89*, 263−273.

17. Tan, K., Liu, J., Wang, J., Shen, S., and Lu, M. (1997) *Proc. Natl. Acad. Sci. U.S.A. 94*, 12303−12308.
18. Caffrey, M., Cai, M., Kaufman, J., Stahl, S. J., Wingfield, P. T., Covell, D. G., Gronenborn, A. M., and Clore, G. M. (1998) *EMBO J. 17*, 4572−4584.
19. Malaskkevich, V. N., Chan, D. C., Chutkowski, C. T., and Kim, P. S. (1998) *Proc. Natl. Acad. Sci. U.S.A. 95*, 9134−9139.
20. Yang, Z.-N., Mueser, T. C., Kaufman, J., Stahl, S. J., Wingfield, P. T., and Hyde, C. C. (1999) *J. Struct. Biol. 126*, 131−144.
21. Jiang, S., Lin, K., and Lu, M. (1998) *J. Virol. 72*, 10213−10217.
22. Ji, H., Bracken, C., and Lu, M. (2000) *Biochemistry 39*, 676−685.
23. Dubay, J. W., Roberts, S. J., Brody, B., and Hunter, E. (1992) *J. Virol. 66*, 4748−4756.
24. Cao, J., Bergeron, L., Helseth, E., Thali, M., Repke, H., and Sodroski, J. (1993) *J. Virol. 67*, 2747−2755.
25. Chen, S. S., Lee, C. N., Lee, W. R., McIntosh, K., and Lee, T. H. (1993) *J. Virol. 67*, 3615−3619.
26. Wild, C. T., Dubay, J. W., Greenwell, T. K., Baird, T., Oas, T. G., McDanal, C. B., Hunter, E., and Matthews, T. J. (1994) *Proc. Natl. Acad. Sci. U.S.A. 91*, 12676−12680.
27. Weng, Y., and Weiss, D. C. (1998) *J. Virol. 72*, 9676−9682.
28. Lu, M., Ji, H., and Shen, S. (1999) *J. Virol. 73*, 4433−4438.
29. Jiang, S., Lin, K., Strick, N., and Neurath, A. R. (1993) *Nature 365*, 113.
30. Wild, C. T., Shugars, D. C., Greenwell, T. K., McDanal, C. B., and Matthews, T. J. (1994) *Proc. Natl. Acad. Sci. U.S.A. 91*, 9770−9774.
31. Kilby, J. M., Hopkins, S., Venetta, T. M., DiMassimo, B., Cloud, G. A., Lee, J. Y., Alldredge, Y., Hunter, E., Lambert, D., Bolognesi, D., Matthews, T., Johnson, M. R., Nowak, M. A., Shaw, G. M., and Saag, M. S. (1998) *Nat. Med. 4*, 1302−1307.
32. Eckert, D. M., Malashkevich, V. N., Hong, L. H., Carr, P. A., and Kim, P. S. (1999) *Cell 99*, 103−115.
33. Ferrer, M., Kapoor, T. M., Strassmaier, T., Weissenhorn, W., Skehel, J. J., Oprian, D., Schreiber, S., Wiley, D. C., and Harrison, S. C. (1999) *Nat. Struct. Biol. 6*, 953−960.
34. Hodges, R. S., Sodek, J., Smillie, L. B., and Jurasek, L. (1972) *Cold Spring Harbor Symp. Quant. Biol. 37*, 299−310.
35. McLachlan, A. D., and Stewart, M. (1975) *J. Mol. Biol. 98*, 293−304.
36. Conway, J. F., and Parry, D. A. (1990) *Int. J. Biol. Macromol. 12*, 328−334.
37. Delwart, E. J., Mosialos, G., and Gilmore, T. (1990) *AIDS Res. Hum. Retroviruses 6*, 703−706.
38. Chambers, P., Pringle, C. R., and Easton, A. J. (1990) *J. Gen. Virol. 71*, 3075−3080.
39. Gallaher, W. R., Ball, J. M., Garry, R. F., Griffin, M. C., and Montelaro, R. C. (1989) *AIDS Res. Hum. Retroviruses 5*, 431−440.
40. Kunkel, T. A., Roberts, J. D., and Zakour, R. A. (1987) *Methods Enzymol. 154*, 367−382.
41. Sambrook, J., Fritsch, E. F., and Maniatis, T. (1989) *Molecular Cloning: A Laboratory Manual*, Cold Spring Harbor Laboratory Press, Cold Spring Harbor, NY.
42. de Jong, J.-J., Goudsmit, J., Keulen, W., Klaver, B., Krone, W., Tersmette, M., and de Ronde, A. (1992) *J. Virol. 66*, 757−765.
43. LaCasse, R. A., Follis, K. E., Moudgil, T., Trahey, M., Binley, J. M., Planelles, V., Zolla-Pazner, S., and Nunberg, J. H. (1998) *J. Virol. 72*, 2491−2495.
44. Tersmette, M., Gruters, R. A., deWolf, F., deGoede, R. E. Y., Lange, J. M. A., Schellekens, P. T. A., Goudsmit, J., Huisman, H. G., and Miedema, F. (1989) *J. Virol. 63*, 2118−2125.
45. York, J., Follis, K. E., Trahey, M., Nyambi, P. N., Zolla-Pazner, S., and Nunberg, J. H. (2001) *J. Virol*. (in press).
46. White-Scharf, M. E., Potts, B. J., Smith, L. M., Sokolowski, K. A., Rusche, J. R., and Silver, S. (1993) *Virology 192*, 197−206.
47. Abacioglu, Y. H., Fouts, T. R., Laman, J. D., Claassen, E., Pincus, S. H., Moore, J. P., Roby, C. A., Kamin-Lewis, R., and Lewis, G. K. (1994) *AIDS Res. Hum. Retroviruses 10*, 371−381.
48. Follis, K. E., Trahey, M., LaCasse, R. A., and Nunberg, J. H. (1998) *J. Virol. 72*, 7603−7608.
49. Hill, C. M., Deng, H., Unutmaz, D., Kewalramani, V. N., Bastiani, L., Gorny, M. K., Zolla-Pazner, S., and Littman, D. R. (1997) *J. Virol. 71*, 6296−6304.
50. Poon, B., Jowett, J. B. M., Stewart, S. A., Armstrong, R. W., Rishton, G. M., and Chen, I. S. Y. (1997) *J. Virol. 71*, 3961−3971.
51. Stamatatos, L., and Cheng-Mayer, C. (1995) *J. Virol. 69*, 6191−6198.
52. Willey, R. L., Martin, M. A., and Peden, K. W. C. (1994) *J. Virol. 68*, 1029−1039.
53. Studier, F. W., Rosenberg, A. H., Dunn, J. J., and Dubendorff, J. W. (1990) *Methods Enzymol. 185*, 60−89.
54. Ji, H., Shu, W., Burling, F. T., Jiang, S., and Lu, M. (1999) *J. Virol. 73*, 8578−8586.
55. Edelhoch, H. (1967) *Biochemistry 6*, 1948−1954.
56. Chen, Y.-H., Yang, J. T., and Chau, K. H. (1974) *Biochemistry 13*, 3350−3359.
57. Cantor, C., and Schimmel, P. (1980) *Biophysical Chemistry*, Freeman, New York.
58. Shu, W., Ji, H., and Lu, M. (1999) *Biochemistry 38*, 5378−5385.
59. Johnson, M. L., Correia, J. J., Yphantis, D. A., and Halvorson, H. R. (1981) *Biophys. J. 36*, 575−588.
60. Laue, T. M., Shah, B. D., Ridgeway, T. M., and Pelletier, S. L. (1992) in *Analytical Ultracentrifugation in Biochemistry and Polymer Science* (Harding, S. E., Rowe, A. J., and Horton, J. C., Eds.) pp 90−125, Royal Society of Chemistry, Cambridge, U.K.
61. Otwinowski, Z., and Minor, W. (1996) *Methods Enzymol. 276*, 307−326.
62. Collaborative Computational Project No. 4 (1994) *Acta Crystallogr. D50*, 760−763.
63. Navaza, J. (1994) *Acta Crystallogr. A50*, 157−163.
64. Brünger, A. T. (1992) *X-PLOR Version 3.1: A system for X-ray Crystallography and NMR*, Yale University Press, New Haven, CT.
65. Jones, T. A., Zou, J.-Y., and Cowan, S. W. (1991) *Acta Crystallogr. A47*, 110−119.
66. Brünger, A. T., Adams, P. D., Clore, G. M., DeLano, W. L., Gros, P., Grosse-Kunstleve, R. W., Jiang, J.-S., Kuszewski, J., Nilges, M., Pannu, N. S., Read, R. J., Rice, L. M., Simonson, T., and Warren, G. L. (1998) *Acta Crystallogr. D54*, 905−921.
67. Laskowski, R. A., MacArthur, M. V., Moss, D. D., and Thornton, J. M. (1993) *J. Appl. Crystallogr. 26*, 283−291.
68. HIV Sequence Database (1998/1999) Los Alamos National Laboratory, Los Alamos, NM.
69. Harbury, P. B., Zhang, T., Kim, P. S., and Alber, T. (1993) *Science 262*, 1401−1407.
70. Lu, M., and Kim, P. S. (1997) *J. Biomol. Struct. Dyn. 15*, 465−471.
71. Crick, F. H. C. (1953) *Acta Crystallogr. 6*, 689−697.
72. LaCasse, R. A., Follis, E., Trahey, M., Scarborough, J. D., Littman, D. R., and Nunberg, J. H. (1999) *Science 283*, 357−362.
73. Skehel, J. L., and Wiley, D. C. (1998) *Cell 95*, 871−874.
74. Shu, W., Liu, J., Ji, H., Radigen, L., Jiang, S., and Lu, M. (2000) *Biochemistry 39*, 1634−1642.
75. Stegmann, T., Delfino, J. M., Richards, F. M., and Helenius, A. (1991) *J. Biol. Chem. 266*, 18404−18410.
76. Tsurudome, M., Gluck, R., Graf, R., Falchetto, R., Schaller, U., and Brunner, J. (1992) *J. Biol. Chem. 267*, 20225−20232.
77. Jelesarov, I., and Lu, M. (2001) *J. Mol. Biol*. (in press).

78. Sattentau, Q. J., and Moore, J. P. (1993) *Philos. Trans. R. Soc. London, Ser. B 342*, 59−66.
79. Sattentau, Q. J., Moore, J. P., Vignaux, F., Traincard, F., and Poignard, P. (1993) *J. Virol. 67*, 7383−7393.
80. Farzan, M., Choe, H., Desjardins, E., Sun, Y., Kuhn, J., Cao, J., Archambault, D., Kolchinsky, P., Koch, M., Wyatt, R., and Sodroski, J. (1998) *J. Virol. 72*, 7620−7625.
81. Binley, J. M., Sanders, R. W., Clas, B., Schuelke, N., Master, A., Guo, Y., Kajumo, F., Anselma, D. J., Maddon, P. J., Olson, W. C., and Moore, J. P. (2000) *J. Virol. 74*, 627−643.
82. Evans, S. V. (1993) *J. Mol. Graphics 11*, 134−138.

BI0024759